

Adaptive Force-based Control for Legged Robots

Yiyu Chen and Quan Nguyen

Abstract—In this paper, we present a novel methodology to introduce adaptive control for force-based control systems, with application to legged robots. In our approach, the reference model is based on the quadratic program force control. We evaluate our proposed control design on a high-fidelity physical simulation of LASER, a dynamic quadruped robot. Our proposed method guarantees input-to-state stability and is successfully validated for the problem of quadruped robots walking on rough terrain while carrying unknown and time-varying loads.

I. INTRODUCTION

Legged robots have great potential for application in disaster and rescue missions. In contrast to wheeled robots, legged robots represent remarkable performance for navigating uneven terrains. Designing and controlling machines to realize these potentials has long motivated work across the legged robotics community and highly-capable quadrupeds (e.g., [10], [15]) begun to assist humans in demanding situations.

Currently, the common control approach for highly dynamic locomotion includes two-dimensional planar simplification [16], which only can be employed for gaits without lateral or roll dynamics; evolutionary optimization for galloping [11], which cannot be solved online with desired frequency; and model predictive control (MPC) approach to determine ground reaction forces and formulate the problem as convex optimization which can be solved under 1 ms [7].

However, all common controllers assume perfect knowledge of the dynamic model. Many time and safety-critical missions such as firefighting, disaster response, exploration, etc. require the robot to operate swiftly and stably while dealing with high levels of uncertainty and large external disturbances. The demand for practical requirement motivates our research on adaptive control for quadruped robots.

A load-carrying scenario is one of the main assistive operations that a legged robot can perform. Recently, some research aimed to achieve this functionality for quadruped by dividing the control system into torso motion control and swing legs control [19], [18]. Then, an adaptive sliding mode control will be added to realize the weight change comes from the external load.

The introduction of the L_1 adaptive control technique has enabled the decoupling of adaptation and robustness in adaptive control techniques. In particular, by applying a low-pass filter as part of the adaptation laws help the L_1 adaptive

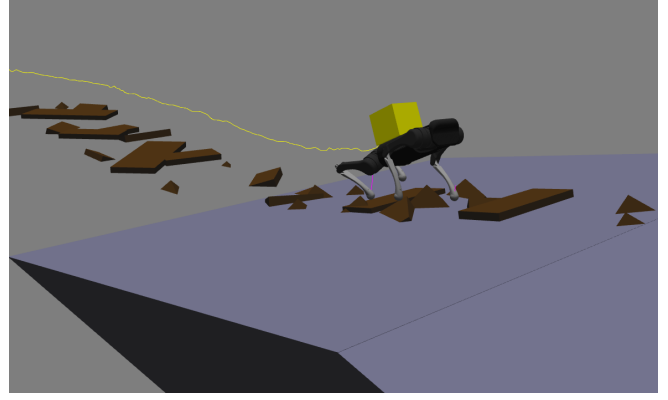


Fig. 1: **The LASER Robot.** The robot walking on high-sloped terrain with obstacles while carrying a 6kg load (50% of body weight) with adaptive control.

controller to guarantee not only stability [4] but also transient performance [5]. Our prior work on L_1 adaptive control for bipedal robots [14] uses a control Lyapunov function (CLF) based controller to create a closed-loop nonlinear reference model for the L_1 adaptive controller. The CLF-base controller can be used for underactuated systems while the quadruped robots are overactuated.

In this paper, we present an adaptive control for nonlinear uncertainty with a reference model that arises from a force-based quadratic program method [8]. The main contribution of the paper is a control system that guarantees input-to-state stability for quadruped robots in presence of uncertainties. Our approach is successfully validated in a high-fidelity simulation for the problem of load-carrying with different scenarios. Although the nominal controller fails to remain the robot in the desired position and orientation, our proposed adaptive controller can satisfy the expectation while carrying an unknown load up to 50% of the robot weight. Thanks to the combination with the forced-base controller, our approach can also allow the robot to navigate rough terrains while carrying an unknown and time-varying load as it is shown in Fig. 1¹.

The remainder of the paper is organized as follows. Sec. II presents an overview of the LASER robot and its hardware information. The force-based control architecture for quadruped robots describes in Sec. III and adaptive controller to compensate uncertainties is elaborated in Sec. IV. Then, the stability proof of the whole system is described in Sec. V. Furthermore, the simulations and results are shown

This work is supported by USC Viterbi School of Engineering startup funds.

Y. Chen, and Q. Nguyen are with the Department of Aerospace and Mechanical Engineering, University of Southern California, Los Angeles, CA 90089, email: yiyuc@usc.edu, quann@usc.edu.

¹Complete video: https://youtu.be/X_jounyuO-M

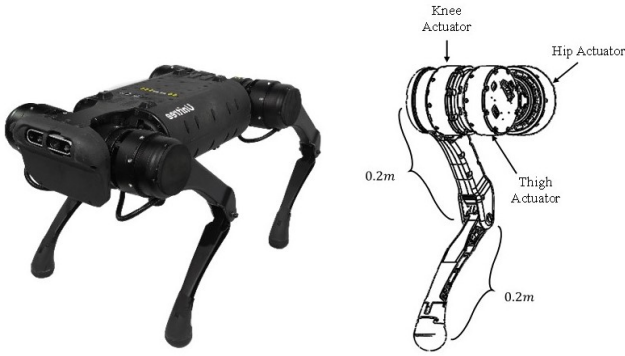


Fig. 2: **Robot Configuration.** Overview of LASER robot and leg configuration

TABLE I: Physical Robot Parameters

Parameter	Symbol	Value	Units
Mass	m	12	kg
Body Inertia	I_{xx}	0.0168	$kg \cdot m^2$
	I_{yy}	0.0565	$kg \cdot m^2$
	I_{zz}	0.0647	$kg \cdot m^2$
Body Length	l_{body}	0.361	m
Body Width	w_{body}	0.194	m
Body Height	h_{body}	0.114	m
Leg Link Lengths	l_1, l_2	0.2	m

in Sec. VI. Finally, Sec. VII provides concluding remarks.

II. ROBOT MODEL

In this paper, we will validate our controller in the model of LASER (Legged-Agile-Smart-Efficient-Robot). The LASER robot is a highly dynamic quadruped platform built from Unitree A1 robot (see Fig. 2). The LASER robot has low-inertial legs and high torque density electric motors with planetary gear reduction, and it is capable of ground force control without using any force or torque sensors. The LASER robot uses these high-performance actuators for all the hip, thigh, and knee joints to enable full 3D control of ground reaction forces. It is also equipped with contact sensors on each foot.

The LASER legs feature a large range of motion as presented in Figure 2. The hip joints have a range of motion of $\pm 46^\circ$, the thigh joints have a range of motion from -60° to 240° and the knee joints have a range from -154.5° to -52.5° . The hip and knee designs allow the robot to operate identically forward, backward and flipped upside-down. The robot parameters are summarized in Table I.

Each of LASER's actuators consists of a custom high torque density electric motor coupled to a single-stage 9:1 planetary gear reduction. The lower link is driven by a bar linkage which passes through the upper link. The legs are serially actuated, but to keep leg inertia low, the hip and knee actuators are co-axially located at the hip of each leg. The actuation capabilities of the LASER robot are summarized in Table II.

TABLE II: Actuator Parameters

Parameter	Value	Units
Gear Ratio	9	
Max Torque	33.5	Nm
Max Joint Speed	21	Rad/s

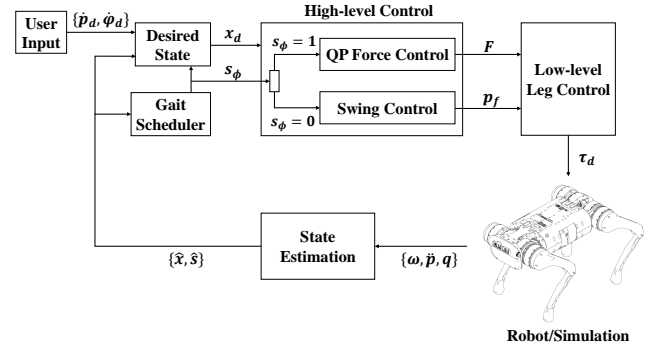


Fig. 3: **Control Architecture Overview.** Block diagram of control architecture for LASER robot.

Having presented the robot hardware, in the next section, we present the background on control of quadruped robots.

III. CONTROL ARCHITECTURE

The control architecture of the robot consists of several modules [2] including high-level controller, low-level controller, state estimation, and gait scheduler as presented in Fig. 3. From user input and state estimation, a reference trajectory can be generated for high-level control. Along with the reference trajectory, the gait scheduler sets up gait timing to switch each leg between swing and stance. Based on the reference trajectory and gait timing, the high-level controller calculates position control for swing legs and force control for stance leg. The low-level leg control converts command generated by high-level control into joint torques and sends it to the robot. Each module of the control architecture will be elaborated in the following sections. The $L1$ adaptive controller is built on this general architecture and will be elaborated in Sec. IV.

A. Gait Scheduler

The LASER's gait is defined by a finite state machine using a leg-independent phase variable to schedule contact and swing phases for each leg [2]. In this paper, a static walking gait is used for a simple QP walking controller and the adaptive walking controller. Independent boolean variables are used to define contact states scheduled $s_\phi \in \{1 = \text{contact}, 0 = \text{swing}\}$, while estimated contacts are defined by $\hat{s}_\phi \in \{1 = \text{contact}, 0 = \text{swing}\}$. With this framework, the robot can switch each leg between swing and stance phases for the controller to execute swing control and force control for each leg.

B. Controller Model

Due to the irregularities of the hybrid nature arising from the repeated contact mode switches as legs enter or leave stance or swing, it is often difficult to use traditional control methods for balancing the robots. Therefore, a simplified control model is used to optimize the ground reaction forces for balancing the whole body motion after impact, enabling a form of real-time optimal controller.

By design, the robot has light limbs with low inertia as compared to the overall body. Therefore, it is reasonable to ignore the effects of the legs into the whole body motion for planning ground reaction forces. In particular, the A1 robot controller model employs a commonly used linear relationship [8], [17] between the body's linear acceleration $\ddot{\mathbf{p}}_c$, angular acceleration $\dot{\boldsymbol{\omega}}_b$, and the forces $\mathbf{F} = (\mathbf{F}_1^T, \mathbf{F}_2^T, \mathbf{F}_3^T, \mathbf{F}_4^T)^T$ acting on each of the robot's four feet. The following linear model is then derived:

$$\underbrace{\begin{bmatrix} \mathbf{I}_3 & \dots & \mathbf{I}_3 \\ [\mathbf{p}_1 - \mathbf{p}_c] \times & \dots & [\mathbf{p}_4 - \mathbf{p}_c] \times \end{bmatrix}}_{\mathbf{A}} \mathbf{F} = \underbrace{\begin{bmatrix} m(\ddot{\mathbf{p}}_c + \mathbf{g}) \\ \mathbf{I}_G \dot{\boldsymbol{\omega}}_b \end{bmatrix}}_{\mathbf{b}}, \quad (1)$$

where m and \mathbf{I}_G are the robot's total mass and centroidal rotational inertia, \mathbf{g} is the gravity vector and $\mathbf{p}_i, i \in \{1, 2, 3, 4\}$ are the positions of the feet. The term $[\mathbf{p}_i - \mathbf{p}_c] \times$ is the skew-symmetric matrix representing the cross product $(\mathbf{p}_i - \mathbf{p}_c) \times \mathbf{F}_i$. The $\mathbf{I}_G \dot{\boldsymbol{\omega}}_b$ is actually an approximation of following equation:

$$\frac{d}{dt}(\mathbf{I}_G \boldsymbol{\omega}_b) = \mathbf{I}_G \dot{\boldsymbol{\omega}}_b + \boldsymbol{\omega}_b \times (\mathbf{I}_G \boldsymbol{\omega}_b) \approx \mathbf{I}_G \dot{\boldsymbol{\omega}}_b \quad (2)$$

The $\boldsymbol{\omega}_b \times (\mathbf{I}_G \boldsymbol{\omega}_b)$ term is small for bodies with small angular velocities and does not contribute significantly to the dynamics of the robot [8]. The \mathbf{b} can be rewritten as

$$\mathbf{b} = \underbrace{\begin{bmatrix} m\mathbf{I}_3 & \mathbf{0} \\ \mathbf{0} & \mathbf{I}_G \end{bmatrix}}_{\mathbf{M}} \underbrace{\begin{bmatrix} \ddot{\mathbf{p}}_c \\ \dot{\boldsymbol{\omega}}_b \end{bmatrix}}_{\mathbf{b}} + \underbrace{\begin{bmatrix} m\mathbf{g} \\ \mathbf{0} \end{bmatrix}}_{\mathbf{G}}. \quad (3)$$

C. Balance Controller

Let the state variable define as $\boldsymbol{\eta} = [\mathbf{e}, \dot{\mathbf{e}}]^T$ which

$$\mathbf{e} = \begin{bmatrix} \mathbf{p}_{c,d} - \mathbf{p}_c \\ \log(\mathbf{R}_d \mathbf{R}^T) \end{bmatrix} \quad (4)$$

and

$$\dot{\mathbf{e}} = \begin{bmatrix} \dot{\mathbf{p}}_{c,d} - \dot{\mathbf{p}}_c \\ \boldsymbol{\omega}_{b,d} - \boldsymbol{\omega} \end{bmatrix} \quad (5)$$

The desired and actual body orientations are described using rotation matrices \mathbf{R}_d and \mathbf{R} , respectively, and the orientation error is obtained using the exponential map representation of rotations [3], [13]. We obtain the closed-loop dynamics in term of $\boldsymbol{\eta}$, as

$$\dot{\boldsymbol{\eta}} = \mathbf{D}\boldsymbol{\eta} + \mathbf{H}\boldsymbol{\mu}, \quad \mathbf{D} = \begin{bmatrix} \mathbf{0} & \mathbf{I} \\ \mathbf{0} & \mathbf{0} \end{bmatrix}, \quad \mathbf{H} = \begin{bmatrix} \mathbf{0} \\ \mathbf{I} \end{bmatrix} \quad (6)$$

then we can apply the PD control

$$\boldsymbol{\mu} = [-\mathbf{K}_P \quad -\mathbf{K}_D] \boldsymbol{\eta} = \begin{bmatrix} \ddot{\mathbf{p}}_{c,d} \\ \dot{\boldsymbol{\omega}}_{b,d} \end{bmatrix}. \quad (7)$$

The goal of the whole controller is to resolve an optimal distribution of leg forces \mathbf{F} that drive the approximate COM dynamics to the corresponding desired dynamics given by

$$\mathbf{b}_d = \mathbf{M}\boldsymbol{\mu} + \mathbf{G}. \quad (8)$$

Since the model (1) is linear, the controller can naturally be expressed as a quadratic program (QP) [9], that can be solved in real-time of 1 kHz:

$$\begin{aligned} \mathbf{F}^* = \min_{\mathbf{F} \in \mathbb{R}^{12}} & (\mathbf{A}\mathbf{F} - \mathbf{b}_d)^T \mathbf{S}(\mathbf{A}\mathbf{F} - \mathbf{b}_d) \\ & + \gamma_1 \|\mathbf{F}\|^2 + \gamma_2 \|\mathbf{F} - \mathbf{F}_{prev}^*\|^2 \\ \text{s.t.} \quad & \mathbf{C}\mathbf{F} \leq \mathbf{d} \\ & \mathbf{F}_{swing}^z = 0 \end{aligned} \quad (9)$$

The cost function in (9) represents three goals: driving the COM to the desired dynamics, minimizing the force commands, and filtering the change of the solution \mathbf{F}^* with respect to the previous time-step, \mathbf{F}_{prev}^* . The weight parameters $\mathbf{S}, \gamma_1, \gamma_2$ reflect the relative priority in different elements. Constraints $\mathbf{C}\mathbf{F} \leq \mathbf{d}$ ensure that the optimized forces stay inside the friction pyramid and that the normal forces lie within feasible bounds.

Based on the contact model coming out from the contact detection, the normal forces of swing legs are constrained to be zeros, $\mathbf{F}_{swing}^z = 0$. Having this constraint in addition to the friction cone constraints in the QP controller, we will enforce the force vectors of the swing legs to be zeros, $\mathbf{F}_{swing} = \mathbf{0}$. The swing legs are then kept at the posing position using PD control described in Sec. III-D until the contact detection in those legs is triggered. Based on this control model, a walking controller with static walking gait is implemented on the robot.

D. Low-level Leg Control

The low-level leg control can generate joint torque command from the ground force and foot position command. For low-level force control, the ground force command is calculated by the controller and transformed to the hip frame by rotation matrix \mathbf{R} . Then, joint torques are calculated from,

$$\boldsymbol{\tau}_i = \mathbf{J}(\mathbf{q})^T \mathbf{F}_i \quad (10)$$

where \mathbf{F}_i is the foot force vector in the hip frame for leg i and $\mathbf{J}(\mathbf{q})$ is the leg Jacobian matrix. For the swing legs, the footstep location for each leg is calculated from corresponding hip location using a linear combination of Raibert heuristic and a feedback term based on velocity [2]. The footstep locations are projected on an assumed ground plane and is calculated by

$$\mathbf{p}_{step,i} = \mathbf{p}_{h,i} + \frac{T_{c\phi}}{2} \dot{\mathbf{p}}_{c,d} + \sqrt{\frac{z_0}{\|\mathbf{g}\|}} (\dot{\mathbf{p}}_c - \dot{\mathbf{p}}_{c,d}) \quad (11)$$

where $T_{c\phi}$ is the stance time scheduled, z_0 is the height of locomotion and $\mathbf{p}_{h,i}$ is the position of the corresponding hip i . A Beizer curve is used to compute the desired swing trajectory for swing legs. To track the desired swing

Define the difference between the real model and the reference model $\tilde{\eta} = \hat{\eta} - \eta$, we then have,

$$\dot{\tilde{\eta}} = D\tilde{\eta} + H\tilde{\mu}_1 + H(\tilde{\alpha}\|\eta\| + \tilde{\beta}), \quad (24)$$

where

$$\tilde{\mu}_1 = \hat{\mu}_1 - \mu_1, \quad \tilde{\alpha} = \hat{\alpha} - \alpha, \quad \tilde{\beta} = \hat{\beta} - \beta. \quad (25)$$

As a result, we will estimate θ indirectly through α and β , or the values of $\hat{\alpha}$ and $\hat{\beta}$ computed by the following adaptation laws based on the projection operators [12],

$$\begin{aligned} \dot{\hat{\alpha}} &= \Gamma \text{Proj}(\hat{\alpha}, y_\alpha), \\ \dot{\hat{\beta}} &= \Gamma \text{Proj}(\hat{\beta}, y_\beta). \end{aligned} \quad (26)$$

where Γ is a symmetric positive definite matrix and the projection functions y_α and y_β are

$$\begin{aligned} y_\alpha &= -H^T P \tilde{\eta} \|\eta\| \\ y_\beta &= -H^T P \tilde{\eta}. \end{aligned} \quad (27)$$

and P will be defined in Sec. V.

V. STABILITY OF PROPOSED SYSTEM

The QP formulation described in (9) always has a solution. Nevertheless, if the desired dynamic vector b_d violates the inequality constraints (such as force limits and friction constraints), the controller provides the optimum value of F^* . Therefore, the corresponding value for b_d and μ can be represented as follows:

$$b^* = AF^* \quad (28)$$

$$\mu^* = M^{-1}(b^* - G). \quad (29)$$

However, we can assume a bounded error for computed dynamic vector

$$\|b^* - b_d\| \leq \delta_b \quad (30)$$

and as a result of (30), we have

$$\|\mu^* - \mu\| \leq \delta_\mu. \quad (31)$$

A. Linear quadratic Lyapunov theory

According to Lyapunov theory [1], the PD control described in (7) will asymptotically stabilize the the system if

$$A_m = \begin{bmatrix} 0 & I \\ -K_P & -K_D \end{bmatrix} \quad (32)$$

is Hurwitz. This means that by choosing a control Lyapunov function candidate as follows

$$V(\eta) = \eta^T P \eta, \quad (33)$$

where P is the solution of the Lyapunov equation $A_m^T P + P A_m = -Q$ (where A_m is defined in (32) and Q is any symmetric positive-definite matrix), we then have

$$\begin{aligned} \dot{V}(\eta, \mu) + \lambda V(\eta) &= \eta^T (D^T P + P D) \eta \\ &+ \lambda V(\eta) + 2\eta^T P H \mu \leq 0 \end{aligned} \quad (34)$$

where,

$$\lambda = \frac{\lambda_{\min}(Q)}{\lambda_{\max}(P)} > 0. \quad (35)$$

The control signal μ^* we construct by solving QP problem (9), is not always the same as μ according to (31). Therefore, it can be rewritten as

$$\mu^* = \mu + \Delta \quad (36)$$

where Δ is the difference causing by QP optimization between the desired PD control signal μ and the real signal μ^* . By substituting (36) in (34), we have,

$$\dot{V}(\eta, \mu^*) + \lambda V(\eta) \leq 2\eta^T P H \Delta \leq \varepsilon_V \quad (37)$$

B. Stability Proof

We consider the following control Lyapunov candidate function

$$\tilde{V} = \tilde{\eta}^T P \tilde{\eta} + \tilde{\alpha}^T \Gamma^{-1} \tilde{\alpha} + \tilde{\beta}^T \Gamma^{-1} \tilde{\beta} \quad (38)$$

therefore, its time derivative will be

$$\begin{aligned} \dot{\tilde{V}} &= \dot{\tilde{\eta}}^T P \tilde{\eta} + \tilde{\eta}^T P \dot{\tilde{\eta}} + \dot{\tilde{\alpha}}^T \Gamma^{-1} \tilde{\alpha} + \tilde{\alpha}^T \Gamma^{-1} \dot{\tilde{\alpha}} \\ &+ \dot{\tilde{\beta}}^T \Gamma^{-1} \tilde{\beta} + \tilde{\beta}^T \Gamma^{-1} \dot{\tilde{\beta}} \end{aligned} \quad (39)$$

in which, we have

$$\begin{aligned} &\dot{\tilde{\eta}}^T P \tilde{\eta} + \tilde{\eta}^T P \dot{\tilde{\eta}} \\ &= (D\tilde{\eta} + H\tilde{\mu}_1 + H\tilde{\alpha}\|\eta\| + H\tilde{\beta})^T P \tilde{\eta} \\ &+ \tilde{\eta}^T P (D\tilde{\eta} + H\tilde{\mu}_1 + H\tilde{\alpha}\|\eta\| + H\tilde{\beta}) \\ &= (D\tilde{\eta} + H\tilde{\mu}_1)^T P \tilde{\eta} + \tilde{\eta}^T P (D\tilde{\eta} + H\tilde{\mu}_1) \\ &+ \tilde{\alpha}^T H^T \|\eta\| P \tilde{\eta} + \tilde{\eta}^T P H \tilde{\alpha} \|\eta\| \\ &+ \tilde{\beta}^T H^T P \tilde{\eta} + \tilde{\eta}^T P H \tilde{\beta} \end{aligned} \quad (40)$$

Because $\tilde{\eta} = \hat{\eta} - \eta$ satisfies the condition imposed by (37), it implies that

$$(H\tilde{\eta} + D\tilde{\mu}_1)^T P \tilde{\eta} + \tilde{\eta}^T P (H\tilde{\eta} + D\tilde{\mu}_1) \leq -\lambda \tilde{\eta}^T P \tilde{\eta} + \varepsilon_{\tilde{V}} \quad (41)$$

Furthermore, with the property of projection operator [12], we have:

$$\begin{aligned} (\hat{\alpha} - \alpha)^T (\text{Proj}(\hat{\alpha}, y_\alpha) - y_\alpha) &\leq 0, \\ (\hat{\beta} - \beta)^T (\text{Proj}(\hat{\beta}, y_\beta) - y_\beta) &\leq 0. \end{aligned} \quad (42)$$

From (26) and (42), we can imply that

$$\begin{aligned} \tilde{\alpha}^T \Gamma^{-1} \dot{\tilde{\alpha}} &\leq \tilde{\alpha}^T y_\alpha - \tilde{\alpha}^T \Gamma^{-1} \dot{\tilde{\alpha}} \\ \dot{\tilde{\alpha}}^T \Gamma^{-1} \tilde{\alpha} &\leq y_\alpha^T \tilde{\alpha} - \dot{\tilde{\alpha}}^T \Gamma^{-1} \tilde{\alpha} \\ \tilde{\beta}^T \Gamma^{-1} \dot{\tilde{\beta}} &\leq \tilde{\beta}^T y_\beta - \tilde{\beta}^T \Gamma^{-1} \dot{\tilde{\beta}} \\ \dot{\tilde{\beta}}^T \Gamma^{-1} \tilde{\beta} &\leq y_\beta^T \tilde{\beta} - \dot{\tilde{\beta}}^T \Gamma^{-1} \tilde{\beta} \end{aligned} \quad (43)$$

We now replace (40), (41) and (43) to (39), which results in

$$\begin{aligned}\dot{\tilde{V}} &\leq -\lambda \tilde{\eta}^T P \tilde{\eta} + \varepsilon_{\tilde{V}} \\ &\quad + \tilde{\alpha}^T (y_\alpha + H^T P \tilde{\eta} \|\eta\|) - \tilde{\alpha}^T \Gamma^{-1} \dot{\alpha} \\ &\quad + (y_\alpha^T + \tilde{\eta}^T P H \|\eta\|) \tilde{\alpha} - \dot{\alpha}^T \Gamma^{-1} \alpha \\ &\quad + \tilde{\beta}^T (y_\beta + H^T P \tilde{\eta}) - \tilde{\beta}^T \Gamma^{-1} \dot{\beta} \\ &\quad + (y_\beta^T + \tilde{\eta}^T P H) \tilde{\beta} - \dot{\beta}^T \Gamma^{-1} \tilde{\beta}\end{aligned}\quad (44)$$

So, by using the chosen projection functions (27), then we conclude that

$$\begin{aligned}\dot{\tilde{V}} + \lambda \tilde{V} &\leq \varepsilon_{\tilde{V}} + \lambda \tilde{\alpha}^T \Gamma^{-1} \tilde{\alpha} + \lambda \tilde{\beta}^T \Gamma^{-1} \tilde{\beta} \\ &\quad - \tilde{\alpha}^T \Gamma^{-1} \dot{\alpha} - \dot{\alpha}^T \Gamma^{-1} \tilde{\alpha} \\ &\quad - \tilde{\beta}^T \Gamma^{-1} \dot{\beta} - \dot{\beta}^T \Gamma^{-1} \tilde{\beta}.\end{aligned}\quad (45)$$

We assume that the uncertainties α , β and their time derivatives are bounded. Furthermore, the projection operators (26) will also keep $\tilde{\alpha}$ and $\tilde{\beta}$ bounded (see [6] for a detailed proof about these properties.) We define these bounds as follows:

$$\begin{aligned}\|\tilde{\alpha}\| &\leq \tilde{\alpha}_b, \quad \|\tilde{\beta}\| \leq \tilde{\beta}_b, \\ \|\dot{\tilde{\alpha}}\| &\leq \dot{\tilde{\alpha}}_b, \quad \|\dot{\tilde{\beta}}\| \leq \dot{\tilde{\beta}}_b.\end{aligned}\quad (46)$$

Combining this with (45), we have,

$$\dot{\tilde{V}} + \lambda \tilde{V} \leq \lambda \delta_{\tilde{V}}, \quad (47)$$

where

$$\delta_{\tilde{V}} = 2\|\Gamma\|^{-1}(\tilde{\alpha}_b^2 + \tilde{\beta}_b^2 + \frac{1}{\lambda}\tilde{\alpha}_b\dot{\tilde{\alpha}}_b + \frac{1}{\lambda}\tilde{\beta}_b\dot{\tilde{\beta}}_b) + \frac{1}{\lambda}\varepsilon_{\tilde{V}}. \quad (48)$$

Thus, if $\tilde{V} \geq \delta_{\tilde{V}}$ then $\dot{\tilde{V}} \leq 0$. As a result, we always have $\tilde{V} \leq \delta_{\tilde{V}}$. In other words, by choosing the adaptation gain Γ and also λ sufficiently large, we can limit the Control Lyapunov Function (38) in an arbitrarily small neighborhood $\delta_{\tilde{V}}$ of the origin. Therefore the tracking errors between the dynamics model (15) and the reference model (17), $\tilde{\eta}$, and the error between the real and estimated uncertainty, $\tilde{\alpha}$, $\tilde{\beta}$ are bounded as follows:

$$\|\tilde{\eta}\| \leq \sqrt{\frac{\delta_{\tilde{V}}}{\|P\|}}, \|\tilde{\alpha}\| \leq \sqrt{\|\Gamma\|\delta_{\tilde{V}}}, \|\tilde{\beta}\| \leq \sqrt{\|\Gamma\|\delta_{\tilde{V}}}. \quad (49)$$

VI. SIMULATION

This section presents the results from high-fidelity simulations to test the adaptive controller on the LASER robot. The control system presented in this paper is implemented in ROS and simulations are performed using Gazebo 9. The robot is simulated to carry a load up to 50% of the robot weight during walking base on the approach we have developed in previous sections. Some snapshots of the simulations are presented in Fig. 5. To demonstrate the effectiveness and performance of the adaptive controller, results are compared for the non-adaptive and adaptive controller.

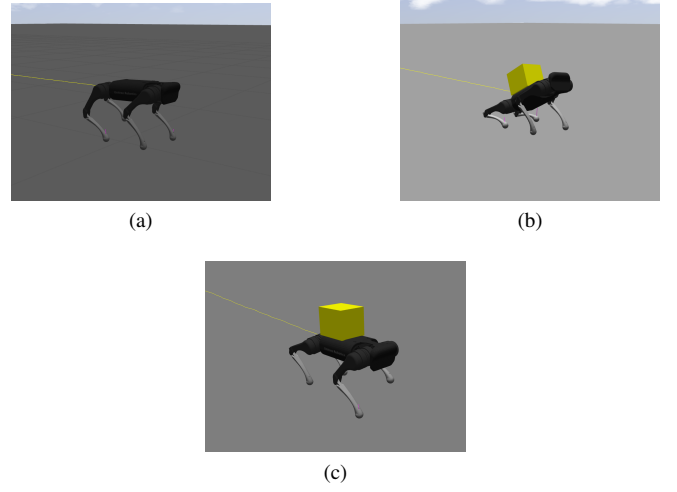


Fig. 5: **Motion Snapshot During Walking** a) Nominal case without uncertainties b) Non-adaptive controller with a load in back c) Adaptive controller with a load in back

A. Nominal Case

First, we simulate the robot without any external load and uncertainties to qualify the performance of the baseline controller. The robot stands up with the QP controller to the height of 0.3m and then switch to the non-adaptive locomotion controller to walk forward with the speed of 0.2 m/s using the static walking gait. This case is used as a reference to compare with the cases with uncertainty in mass and inertia.

B. Uncertainty in Mass and Inertia

Next, the 6kg load is applied to the back of the robot to create uncertainty in mass and inertia, simultaneously. The results of the non-adaptive controller and the adaptive controller for this case are shown in Fig. 6. Since our simulation does not emphasize the significant difference in tracking errors of position along the x-axis, y-axis, roll and yaw angles, we select to show plots of tracking errors in z-axis and pitch angle.

By comparing plots in Fig. 6, it can be obtained that the baseline controller cannot compensate for the uncertainties and the results are improved by using adaptive controller. Although we have a constant error for the adaptive controller, it does not contradict with the algorithm we have developed, because the controller system we have designed guarantees the input-to-state stability.

C. Varying Load

Finally, a 2kg load is applied to the back of the robot and a time-varying force is applied to the robot body during the motion (after 2 seconds from starting point). The value of external force with the tracking error along the z-axis and pitch angle are presented in Fig. 7. These plots are results of using the adaptive controller to demonstrate its stability.

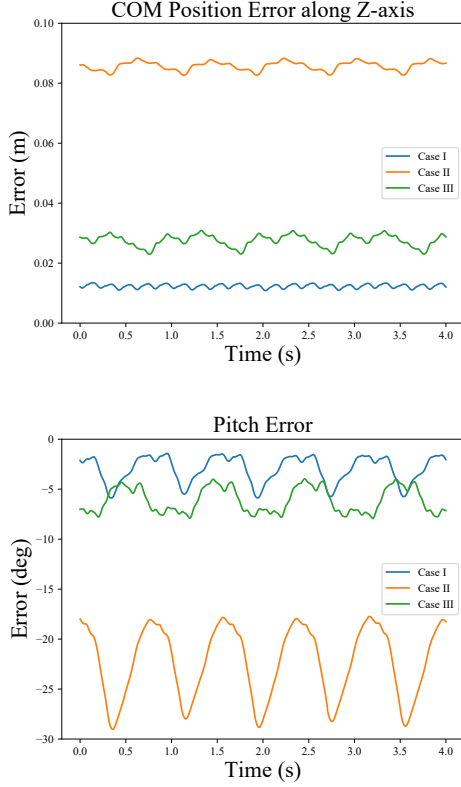


Fig. 6: **Plots of nominal case and load-carrying results.** Case I: Nominal case without uncertainties; Case II: Non-adaptive controller with a load in back; Case III: Adaptive controller with a load in back

VII. CONCLUSION

In summary, we have presented a control method to apply L_1 adaptive control for dynamic legged robot walking under uncertainties. The controller explicitly considers the nonlinear, overactuated, and hybrid dynamics that are characteristic of quadruped robots. The proposed control system uses a quadratic program optimization-based controller to create a closed-loop nonlinear reference model for the L_1 adaptive controller for working in the presence of uncertainty. Numerical simulations on LASER demonstrate the validity of the proposed controller in order to track nonlinear reference dynamics under the presence of a high level of uncertainty.

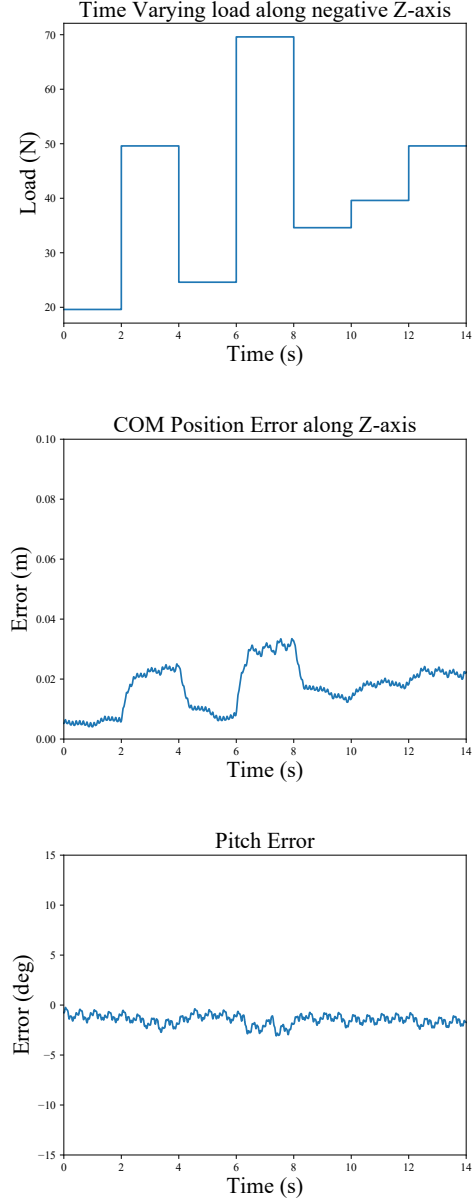


Fig. 7: **Plots of carrying a time-varying load using adaptive controller**

REFERENCES

- [1] A. D. Ames, K. Galloway, J. W. Grizzle, and K. Sreenath, "Rapidly Exponentially Stabilizing Control Lyapunov Functions and Hybrid Zero Dynamics," *IEEE Trans. Automatic Control*, 2014.
- [2] G. Bledt, M. J. Powell, B. Katz, J. Di Carlo, P. M. Wensing, and S. Kim, "Mit cheetah 3: Design and control of a robust, dynamic quadruped robot," in *2018 IEEE/RSJ International Conference on Intelligent Robots and Systems (IROS)*. IEEE, 2018, pp. 2245–2252.
- [3] F. Bullo and R. M. Murray, "Proportional derivative (PD) control on the Euclidean group," in *Proc. of the European Control Conference*, Rome, Italy, Jun. 1995, pp. 1091–1097.
- [4] C. Cao and N. Hovakimyan, "Stability margins of l1 adaptive controller: Part ii," *Proceedings of American Control Conference*, pp. 3931–3936, 2007.
- [5] —, "Design and analysis of a novel l1 adaptive controller with guaranteed transient performance," *IEEE Transactions on Automatic Control*, vol. 53, no. 2, pp. 586–591, March, 2008.
- [6] C. Cao and N. Hovakimyan, "L1 adaptive controller for a class of systems with unknown nonlinearities: Part i," *American Control Conference, Seattle, WA*, pp. 4093–4098, 2008.
- [7] J. Di Carlo, P. M. Wensing, B. Katz, G. Bledt, and S. Kim, "Dynamic locomotion in the mit cheetah 3 through convex model-predictive control," in *2018 IEEE/RSJ International Conference on Intelligent Robots and Systems (IROS)*. IEEE, 2018, pp. 1–9.
- [8] M. Focchi, A. del Prete, I. Havoutis, R. Featherstone, D. G. Caldwell, and C. Semini, "High-slope terrain locomotion for torque-controlled quadruped robots," *Autonomous Robots*, vol. 41, no. 1, pp. 259–272, Jan 2017. [Online]. Available: <https://doi.org/10.1007/s10514-016-9573-1>
- [9] C. Gehring, S. Coros, M. Hutter, M. Bloesch, M. Hoepflinger, and R. Siegwart, "Control of dynamic gaits for a quadrupedal robot," in *IEEE International Conference on Robotics and Automation (ICRA)*, May 2013, pp. 3287–3292.
- [10] M. Hutter, C. Gehring, D. Jud, A. Lauber, C. D. Bellicoso, V. Tsounis, J. Hwangbo, K. Bodie, P. Fankhauser, M. Bloesch, R. Diethelm, S. Bachmann, A. Melzer, and M. Hoepflinger, "ANYmal - a highly mobile and dynamic quadrupedal robot," in *IEEE/RSJ International Conference on Intelligent Robots and Systems*, Oct 2016, pp. 38–44.
- [11] D. P. Krasny and D. E. Orin, "Evolution of a 3d gallop in a quadrupedal model with biological characteristics," *Journal of Intelligent & Robotic Systems*, vol. 60, no. 1, pp. 59–82, 2010.
- [12] E. Lavretsky, T. E. Gibson, and A. M. Annaswamy, "Projection operator in adaptive systems," *arXiv:1112.4232v6*, 2012.
- [13] R. M. Murray, Z. Li, and S. S. Sastry, *A Mathematical Introduction to Robotic Manipulation*. CRC Press, 1994.
- [14] Q. Nguyen and K. Sreenath, "L1 adaptive control for bipedal robots with control lyapunov function based quadratic programs," in *2015 American Control Conference (ACC)*. IEEE, 2015, pp. 862–867.
- [15] H.-W. Park, P. Wensing, and S. Kim, "Online planning for autonomous running jumps over obstacles in high-speed quadrupeds," in *Proceedings of Robotics: Science and Systems*, Rome, Italy, July 2015.
- [16] H.-W. Park, P. M. Wensing, and S. Kim, "High-speed bounding with the mit cheetah 2: Control design and experiments," *The International Journal of Robotics Research*, vol. 36, no. 2, pp. 167–192, 2017.
- [17] B. Stephens and C. Atkeson, "Push recovery by stepping for humanoid robots with force controlled joints," in *IEEE-RAS International Conference on Humanoid Robots*, Dec. 2010, pp. 52–59.
- [18] Y. Tan, Z. Chao, S. Han, H. Li, and X. Liu, "Trotting control of load-carrying quadruped walking vehicle with load variations based on the centroidal dynamics and adaptive sliding mode control," *Mathematical Problems in Engineering*, vol. 2020, 2020.
- [19] Y. Tan, Z. Chao, H. Li, S. Han, and Y. Jin, "Control of trotting gait for load-carrying quadruped walking vehicle with eccentric torso," *International Journal of Advanced Robotic Systems*, vol. 17, no. 4, p. 1729881420931676, 2020.